The k-filtering technique applied to wave electric and magnetic field measurements from the Cluster satellites.

Anders Tjulin, Jean-Louis Pinçon, Fouad Sahraoui, Mats André, Nicole Cornilleau-Wehrlin

The k-filtering technique applied to wave electric and magnetic field measurements from the Cluster satellites

Anders Tjulin[1] and Jean-Louis Pinçon
LPCE/CNRS, Orléans, France

Fouad Sahraoui[2] and Mats André
Swedish Institute of Space Physics, Uppsala, Sweden

Nicole Cornilleau-Wehrlin
CETP/IPSL, Vélizy, France

Received 8 March 2005; revised 27 August 2005; accepted 26 September 2005; published 30 November 2005.

[1] The k-filtering technique is a method to characterize stationary fluctuations in space plasmas in terms of the wave energy distribution in the frequency and wave vector space. It has the ability to distinguish between wave modes of the same frequency in the spacecraft frame of reference, but with different wave vectors. This method is based on simultaneous multi-point measurements of the wave field components, where a filter bank is used to enhance the spatial resolution. We have for the first time combined electric field data from the Electric Field and Wave (EFW) instrument and magnetic field data from the Spatio-Temporal Analysis of Field Fluctuation (STAFF) instrument on the four Cluster spacecraft in order to determine the wave energy distribution. The k-filtering technique has previously been performed with only the magnetic field measurements. The reason to include the electric field measurements is that it is important to include as much data as possible in order to get the best possible estimation of the wave energy distribution. Another reason is that it also enables comparisons between the electric and the magnetic part of the wave energy distribution to make it possible to differentiate the observed waves according to their polarization. The k-filtering method has been extended in order to allow for two measured components of the electric field, and also for the possibility that the electric field measurements from one or more satellites cannot be used for k-filtering. The technique has been applied on satellite data from the magnetosheath and the foreshock, and from these examples it is clear that k-filtering using both electric and magnetic field measurements is a good tool for characterizing the waves that are observed in space.

Citation: Tjulin, A., J.-L. Pinçon, F. Sahraoui, M. André, and N. Cornilleau-Wehrlin (2005), The k-filtering technique applied to wave electric and magnetic field measurements from the Cluster satellites, *J. Geophys. Res.*, *110*, A11224, doi:10.1029/2005JA011125.

1. Introduction

[2] Waves are ubiquitous in space plasmas. They mediate the transport of energy between different parts of space as well as between different particles in the plasma medium. The polarization and the dispersive properties of the waves are not arbitrary, but depend on the properties of the plasma. This makes the identification of observed waves important, since the comparison between the observations and the theoretically predicted behaviour of the waves then provides information about the source of the waves as well as the plasma medium in which these waves propagate. The proper identification of the observed waves is thus a good tool for understanding the space plasma environment.

[3] The plasma wave mode identification has historically mostly been limited to observations from a single spacecraft. The basis for this kind of single-point analysis is observations of the relationship between the measured physical parameters of the wave. This is expressed in terms of a number of dimensionless parameters, such as polarization and transport ratios [e.g., *Schwartz et al.*, 1996]. Comparisons between observations and analytically or numerically found expressions, derived from plasma models, are consequently performed to determine which plasma wave mode is observed. The Wave Distribution Function

[1]Now at Imperial College, London, UK.
[2]Now at CETP/IPSL, Vélizy, France.

0148-0227/05/2005JA011125

(WDF) technique [e.g., *Storey and Lefeuvre*, 1979; *Stenberg et al.*, 2002] is another method for investigating the wave field in a plasma using single spacecraft measurements. These approaches are limited by the fact that they depend on the choice of plasma model for the determination of the wave vector, **k**. The dispersive properties of the waves can thus not directly be observed using this kind of analysis. Another problem is that all observed wave frequencies are in the spacecraft frame of reference. When the wave vector is not known, it is difficult to estimate the frequency in a reference frame at rest with respect to the plasma, and that is the relevant frequency in most theories.

[4] It is possible to estimate the projection of the wave vector along the separation axis between two closely separated spacecraft. This is done by using the phase difference of the waves observed by the two spacecraft to estimate the phase velocity of the waves [e.g., *Dudok de Wit et al.*, 1995]. This method is often called the phase difference method, and it is applicable under the assumption that the inter-spacecraft separation distance is smaller than the wavelength of the observed wave. In order to get the full three-dimensional wave vector with this method, we need to simultaneously know the phase differences along three spacecraft separation axes that are not lying in the same plane, and that means that we need observations from at least four different points in space. In addition, this method depends, as most other multi-spacecraft analysis techniques, on the assumption of plane waves [*Dunlop et al.*, 1988]. One wave vector for each measured frequency can be robustly estimated this way, but the polarization of the waves, that is the relation between the different wave components, is not explicitly included in the method, which it should be in order to accurately identify the wave modes. Another method, based on the Hilbert transform, has also been introduced [*Carozzi et al.*, 2004] which determines the instantaneous wave vector and frequency of the observed wave. This method thus enables investigations of non-stationary wave data but it still cannot distinguish between two wave modes, if they have the same frequency in the spacecraft frame of reference.

[5] The k-filtering technique is essentially a three-dimensional generalization to space plasmas of a method to analyze seismological data [*Capon*, 1969]. This technique was introduced by *Pinçon and Lefeuvre* [1991] and it includes observations of the wave polarization from multiple spacecraft for the estimation of the wave field energy distribution, P, as a function of the frequency and the wave vector. The fact that the output of this method is an energy distribution, rather than just a single number, enables the finding of more than one wave field energy maximum at each measured frequency. This method can thus, in contrast to the previous methods, be used for wave mode identification in plasmas where several wave modes may occur at each frequency. This is a very important advantage of the k-filtering technique over other methods, since space plasmas usually contain a large number of wave modes that may have the same frequency. It is also not possible to claim that there is only one wave mode present at each frequency without having the means to verify that.

[6] Following the launch of the four ESA Cluster satellites [*Escoubet et al.*, 1997], these multi-point techniques can be applied routinely, at least as long as the spacecraft constellation is close to a regular tetrahedron. The first study using the k-filtering method on real space data was performed by *Glassmeier et al.* [2001]. In a later study performed by *Sahraoui et al.* [2003, 2004], the k-filtering technique was applied on Cluster measurements of the wave magnetic field in order to analyze the plasma wave turbulence in the Earth's magnetosheath. The conclusion was that the low frequency part of the observed spectrum was dominated by the mirror mode that had been Doppler shifted. The same data-set was also used in a comparative study between the results obtained by the phase-differencing and by the k-filtering methods [*Walker et al.*, 2004]. The conclusion from this comparison was that the k-filtering technique requires a longer time series, compared to the phase-differencing method, but that it is instead able to find several different wave modes at the same frequency, just as expected.

[7] Most multi-point wave studies so far have been performed using wave magnetic data. The purpose of this study is to include the electric field measurements in the k-filtering framework in order to utilize a larger part of the electromagnetic fluctuations in the analysis. Section 2 describes the basic ideas of the k-filtering method. The Cluster instruments that are used in this study are described in section 3, and section 4 outlines how the equations of the k-filtering technique can be adjusted in order to accurately include the Cluster electric field measurements. A discussion of the accuracy of the method is found in section 5, followed by two examples where the described method has been applied on Cluster data in section 6. The conclusions from this study can be found in section 7. Finally, Appendix A includes a couple of analytical examples to point out some precautions to take when interpreting the results of the k-filtering method.

2. Basics of k-Filtering

[8] The k-filtering technique is a multi-spacecraft method to estimate the wave field energy distribution, P, as a function of angular frequency, ω, and wave vector, **k**. The basic idea of k-filtering is to apply a filter bank in the spatial domain to a data time series that is measured at several spatial locations and has been transformed into frequency domain [*Pinçon and Lefeuvre*, 1991]. This specific filter is dependent on ω and **k**, and it is ideally designed in such a way that it absorbs all wave field energy except the part that is corresponding to plane waves with ω and **k**, which should pass the filter undisturbed. In this text we will use the notation of *Pinçon and Motschmann* [1998], and this notation is introduced before the k-filtering method itself is presented.

[9] Let $\mathbf{A}(\mathbf{r}, t)$ be the measured time-series of the wave field, consisting of L quantities, at the spatial point **r**. We assume that we are observing a superposition of plane waves, and we will here use the following convention:

$$\mathbf{A}(\mathbf{r},t) = \mathrm{Re}\left[\sum_{\omega}\sum_{\mathbf{k}}\mathbf{A}(\omega,\mathbf{k})e^{i(\mathbf{k}\cdot\mathbf{r}-\omega t)}\right]. \quad (1)$$

The wave field energy distribution, $P(\omega, \mathbf{k})$, is given by the trace of the spectral wave field energy matrix, $\mathbf{P}(\omega, \mathbf{k})$. This matrix is defined by

$$\mathbf{P}(\omega,\mathbf{k}) = \left\langle \mathbf{A}(\omega,\mathbf{k})\mathbf{A}^{\dagger}(\omega,\mathbf{k})\right\rangle, \quad (2)$$

where † denotes the adjoint operation, and the brackets a time average. The k-filtering technique is a convenient method to estimate this distribution from measured data.

[10] The frequency dependence of the time-series can easily be found by Fourier transformation. This immediately enables us to go into frequency domain where we express the measured wave field as $\mathbf{A}(\omega, \mathbf{r})$. The measured wave fields from the N different spacecraft, at positions $\mathbf{r}_i$, are then assembled in a single vector $\mathbf{A}(\omega)$, which is defined by

$$\mathbf{A}(\omega) = \begin{pmatrix} \mathbf{A}(\omega, \mathbf{r}_1) \\ \mathbf{A}(\omega, \mathbf{r}_2) \\ \vdots \\ \mathbf{A}(\omega, \mathbf{r}_N) \end{pmatrix}. \tag{3}$$

From this vector we define the spatial correlation matrix, $\mathbf{M}(\omega)$ in order to keep track of the amplitudes and the relative phase differences between the different measured physical quantities, as well as the different satellites. It is defined as:

$$\mathbf{M}(\omega) = \left\langle \mathbf{A}(\omega)\mathbf{A}^{\dagger}(\omega) \right\rangle. \tag{4}$$

The averaging in this expression means that we need a rather long time period where the time-series is stationary for the calculation of the spatial correlation matrix. If we for example want a frequency resolution corresponding to a 1024 point FFT of the time series, we typically need at least four times as many points to make a reasonable average, i.e. 4096 data points.

[11] We also need to include the positions of the spacecraft in this framework. This is done by introducing the matrix $\mathbf{H}(\mathbf{k})$, which is defined by

$$\mathbf{H}(\mathbf{k}) = \begin{pmatrix} \mathbf{I}_{\mathbf{L}} e^{i\mathbf{k}\cdot\mathbf{r}_1} \\ \mathbf{I}_{\mathbf{L}} e^{i\mathbf{k}\cdot\mathbf{r}_2} \\ \vdots \\ \mathbf{I}_{\mathbf{L}} e^{i\mathbf{k}\cdot\mathbf{r}_N} \end{pmatrix}, \tag{5}$$

where $\mathbf{I}_{\mathbf{L}}$ is the $L \times L$ unit matrix. L is, as mentioned before, the number of measured components of the wave field, and N the number of spacecraft.

[12] It can be shown that the final expression for the wave field energy distribution, when the filter bank is applied to the measured data, can be written [*Pinçon and Lefeuvre*, 1991; *Pinçon and Motschmann*, 1998]

$$P(\omega, \mathbf{k}) = \mathrm{Tr}\left\{ \left(\mathbf{H}^{\dagger}(\mathbf{k})\mathbf{M}^{-1}(\omega)\mathbf{H}(\mathbf{k}) \right)^{-1} \right\}. \tag{6}$$

This is the basic equation of k-filtering. Some analytical examples of the use of this expression are given in Appendix A. The measured components of the field can often be described using a smaller set of components, using for example Maxwell's equations. In those cases, we have additional requirements on the wave field which can be included in the k-filtering technique in the form of a constraining matrix $\mathbf{C}(\mathbf{k}, \omega)$. It can be shown [*Pinçon and Lefeuvre*, 1991; *Pinçon and Motschmann*, 1998] that the expression for the spectral wave field energy distribution is changed to

$$P(\omega, \mathbf{k}) = \mathrm{Tr}\left\{ \mathbf{C}\left(\mathbf{C}^{\dagger}\mathbf{H}^{\dagger}\mathbf{M}^{-1}\mathbf{H}\mathbf{C} \right)^{-1} \mathbf{C}^{\dagger} \right\}, \tag{7}$$

when the additional constraints are included. These added constraints are important since they enhance the capabilities of the k-filtering technique by also involving the polarization, the relation between the different components of the observed wave field. Some examples of different constraining matrices are given in section 4.

[13] The k-filtering technique can be considered as a method to decompose the total measured spatial correlation matrix $\mathbf{M}(\omega)$ into a sum of correlation matrices, corresponding to pure plane wave modes. Since $\mathbf{M}(\omega)$ is an $NL \times NL$ matrix, it can only be decomposed into NL linearly independent correlation matrices [e.g., *Samson*, 1983]. One of these matrices corresponds to the incoherent noise in the data, which leaves us with a theoretical maximum of $NL - 1$ different wave modes that can be distinguished using the k-filtering method. This limit of the method is shown in the analytical examples in Appendix A. By measuring more components of the wave field, we may distinguish between a larger number of wave modes. Using a larger number of satellites will also help, since the number of wave modes depends on the size of the measured spatial correlation matrix. The use of constraints on the field components will on the other hand reduce the number of wave modes, since they reduce the number of independent components of the wave field.

[14] A time-series of data should always be filtered before sampling so that aliasing effects do not occur in the dataset. The same is true for sampling a "space-series" at different positions in space, but this is not possible. Instead we encounter the phenomenon that is called spatial aliasing. Its effects can for example be seen in all the analytical examples in Appendix A. The basic unit for examining this effect is a spacecraft pair, which we describe by the separation vector, $\mathbf{r}_{ij} = \mathbf{r}_i - \mathbf{r}_j$, between the two spacecraft (i and j) of the pair. The use of exponential functions to describe the waves, equation (1), makes us investigate the periodicity of this function. We know $\exp\{i\mathbf{k}\cdot\mathbf{r}_{ij}\} = \exp\{i(\mathbf{k} + \Delta\mathbf{k})\cdot\mathbf{r}_{ij}\}$, if $\Delta\mathbf{k}\cdot\mathbf{r}_{ij} = 2\pi n_{ij}$ as long as n_{ij} is an integer. This means that the spacecraft pair with $\mathbf{r}_{ij}$ as a separation vector cannot distinguish between waves with wave vector $\mathbf{k}$ and $\mathbf{k} + \Delta\mathbf{k}$. Two wave modes that cannot be distinguished by any spacecraft pair must then differ by a $\Delta\mathbf{k}$ that satisfies each one in the following set of $N(N-1)/2$ equations:

$$\Delta\mathbf{k}\cdot\mathbf{r}_{ij} = 2\pi n_{ij}, \qquad 1 \le i < j \le N. \tag{8}$$

The general solution to this problem for arbitrary N is typically rather difficult to find.

[15] The solution to equation (8) can in the case of four satellites, as in the Cluster mission, be written in a simple form [*Neubauer and Glassmeier*, 1990]:

$$\Delta\mathbf{k} = n_{14}\Delta\mathbf{k}_1 + n_{24}\Delta\mathbf{k}_2 + n_{34}\Delta\mathbf{k}_3, \tag{9}$$

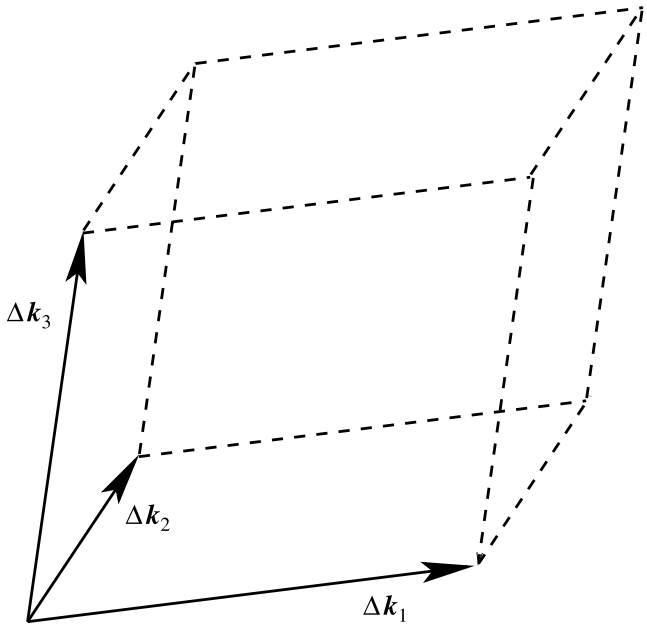

Figure 1. The parallelepiped in *k*-space that is used for describing the spatial aliasing properties. A wave with a wave vector inside this region can not give rise to an aliased peak anywhere else inside this region. Waves with wave vectors outside of this region may however do that.

where we have

$$\begin{aligned}\Delta\mathbf{k}_1 &= 2\pi\mathbf{r}_{24}\times\mathbf{r}_{34}/V\\ \Delta\mathbf{k}_2 &= 2\pi\mathbf{r}_{34}\times\mathbf{r}_{14}/V\\ \Delta\mathbf{k}_3 &= 2\pi\mathbf{r}_{14}\times\mathbf{r}_{24}/V,\end{aligned} \tag{10}$$

and

$$V = \mathbf{r}_{14}\cdot[\mathbf{r}_{24}\times\mathbf{r}_{34}]. \tag{11}$$

Here $|V|$ is the volume of the parallelepiped spanned by the spacecraft separation vectors $\mathbf{r}_{14}$, $\mathbf{r}_{24}$ and $\mathbf{r}_{34}$. The volume of the tetrahedron that the four spacecraft form is $|V|/6$.

[16] The region in *k*-space that is centered on $\mathbf{k} = \mathbf{0}$, which is given by

$$\mathbf{k} = \nu_1\Delta\mathbf{k}_1 + \nu_2\Delta\mathbf{k}_2 + \nu_3\Delta\mathbf{k}_3, \tag{12}$$

with $-1/2 \le \nu_{1,2,3} < 1/2$, is the one of most interest for us. This region is shown in Figure 1, and a wave with a wave vector inside this region does not give rise to any aliased peak anywhere else within this region. This parallelepiped is used in section 6 for the visualization the spatial aliasing properties.

[17] We may note that this discussion of the spatial aliasing problem is valid for all interferometric methods to find wave vectors, using the plane wave assumption. The k-filtering method can, however, suppress the aliased peaks in the wave field energy distribution by convenient choice of a constraining matrix. This can be done more efficiently when more components of the wave field are measured. The spatial configuration of the spacecraft is clearly important for the applicability of the k-filtering method. In order to have the same resolution and aliasing properties for all directions in *k*-space, the spacecraft are ideally positioned at the vertices of a regular tetrahedron.

3. The Instruments and the Data

[18] The data that are used in this analysis come from the Cluster satellite mission [*Escoubet et al.*, 1997]. This mission consists of four identical spacecraft flying in formation with a polar orbit that has perigee at 19,000 km and apogee at 119,000 km, which allows four-point measurements in a wide variety of plasma environments. Each spacecraft is spinning at a rate of 0.25 Hz, with a spin axis close to the $-z$-direction in the Geocentric Solar Ecliptic (GSE) coordinate system. The wave magnetic field data we use here are collected by the Spatio-Temporal Analysis of Field Fluctuations (STAFF) instrument [*Cornilleau-Wehrlin et al.*, 1997], and the electric field measurements come from the Electric Field and Wave (EFW) instrument [*Gustafsson et al.*, 1997]. Both instruments were sampling in the standard operation mode in the presented examples which means that they both sample a 10 Hz low-pass filtered time-series with 25 samples/s.

[19] The STAFF instrument measures all three wave magnetic field components using search coils. A high-pass filter at 0.1 Hz is first applied in order to remove low-frequency artefacts in the search coil data. Then the data are transformed into a non-spinning coordinate system and finally they are high-pass filtered again. This time at 0.35 Hz. The last step is performed in order to remove possible satellite spin effects from the measured time series.

[20] The EFW instrument consists of two pairs of spherical probes where each probe is mounted on a 44 m wire boom. This means that only the two electric field components in the spin plane can be measured by EFW, and this fact has to be taken into account when the EFW electric field data are included in the k-filtering. Another potential source of problems is that there have been failures of one of the EFW probes on each of spacecraft 1 (28/12/2001) and spacecraft 3 (29/07/2002), which prevents the electric field data from the affected satellites to be useful for k-filtering analysis. After 29 September 2003 the EFW instruments on these two satellites are run so that the electric field in the spin plane can be obtained from three probes, which means electric field data from all four satellites can be used again after this date. The k-filtering equations thus have to be adjusted to include three magnetic and two electric field components, but with the possible lack of electric field data from one or more satellites.

[21] The process of removing the effects of the satellite spin from the data cannot be made as directly for the EFW measurements as in the case of STAFF data. This is due to the fact that the EFW measurement of an electric field component involves a probe pair where the two probes are separated by 88 m, while the STAFF measurement of a magnetic field component is essentially a one-point measurement. The spacecraft induced asymmetry of the plasma around the satellite, originating from wake effects or photo-electrons [e.g., *Pedersen et al.*, 1998], may result in a situation where the two probes in a pair are situated in slightly different plasma environments

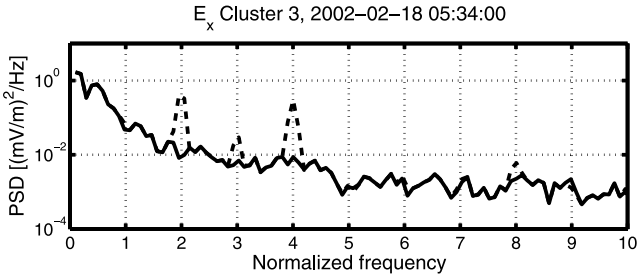

Figure 2. Power spectral density of the sunward component of the electric field measured by Cluster spacecraft 3 at 18 February 2002, 05:34:00–05:36:44 UT. The solid line denotes data that are cleaned according to section 3 and the dashed line data that are not cleaned. The frequency scale is normalized to the spacecraft spin frequency (0.25 Hz). See color version of this figure in the HTML.

during parts of the satellite spin. This will give rise to a periodic disturbance in the measured electric field with a period equal to the spacecraft spin period, which also contains higher harmonics of the spin frequency since the disturbance is not sinusoidal. It is thus not possible to remove the effects of the satellite spin simply by using a high-pass filter on the time series. Instead other methods have to be used.

[22] The electric field data in the present analysis have been cleaned of satellite spin effects by considering the measured electric field as a function of the spacecraft phase angle, a description of its orientation during the spin period, instead of as a function of time. By making a high-pass filtering of this "phase angle series", we can conveniently remove the exact spin frequency and its lowermost harmonics without affecting the rest of the data. We then return the filtered data set to the form of a time series, and continue the analysis with these data. This procedure is comparable to applying a series of very narrow-band notch filters, at the spin frequency and its lowest harmonics, to the time-series. Our method is however more suitable in this situation since the spin frequency has to be known with very high precision in order to obtain the same result with the notch filters. A comparison between cleaned and uncleaned electric field data is shown in Figure 2, from which we see that the general shape of the spectrum is retained but the peaks at the satellite spin frequency harmonics are removed.

[23] The described cleaning of the electric field data is ideally performed using a large number of spacecraft rotations in order to keep its influence on other frequencies down. The plasma conditions must thus be stationary during the time period for these rotations. This is not a problem for the present use of the electric field data, since the k-filtering method already has a stationarity condition on the wave field for its applicability. A time interval that is suitable for k-filtering is hence also suitable for this data cleaning procedure. The drawback with the procedure is that the information about a possible constant background electric field is also removed by the filtering. That information is however not relevant in this analysis.

[24] It is important that all the data used for k-filtering are on the same time-line, as noted by *Pinçon and Motschmann* [1998]. The data collection of the STAFF and the EFW instruments on Cluster are synchronized on each satellite, and the time differences between the satellites are also known to great precision. This makes the conversion to a common time-line easy, especially since we will be working in the frequency domain henceforth and thus only need to study one frequency at a time. The synchronisation is performed by multiplying the data with the appropriate phase factor in frequency domain.

4. K-Filtering With STAFF and EFW Data

[25] The components of the electromagnetic field are not independent. They are instead subject to constraints such as Faraday's law. This constraint enables the construction of all six components of the electromagnetic field from the three electric field components. In the k-filtering notation we use here, this constraint can be written [*Pinçon and Lefeuvre*, 1991]

$$\begin{pmatrix} E_x(\omega,\mathbf{k}) \\ E_y(\omega,\mathbf{k}) \\ E_z(\omega,\mathbf{k}) \\ cB_x(\omega,\mathbf{k}) \\ cB_y(\omega,\mathbf{k}) \\ cB_z(\omega,\mathbf{k}) \end{pmatrix} = \begin{pmatrix} 1 & 0 & 0 \\ 0 & 1 & 0 \\ 0 & 0 & 1 \\ 0 & -\frac{ck_z}{\omega} & \frac{ck_y}{\omega} \\ \frac{ck_z}{\omega} & 0 & -\frac{ck_x}{\omega} \\ -\frac{ck_y}{\omega} & \frac{ck_x}{\omega} & 0 \end{pmatrix} \begin{pmatrix} E_x(\omega,\mathbf{k}) \\ E_y(\omega,\mathbf{k}) \\ E_z(\omega,\mathbf{k}) \end{pmatrix} = \mathbf{C_1}(\omega,\mathbf{k}) \begin{pmatrix} E_x(\omega,\mathbf{k}) \\ E_y(\omega,\mathbf{k}) \\ E_z(\omega,\mathbf{k}) \end{pmatrix}. \quad (13)$$

The matrix $\mathbf{C_1}(\omega, \mathbf{k})$ above is an example of the constraining matrix that was used in equation (7), and c is the speed of light, which is introduced in the equations in order for all elements of the constraining matrix to be of unit dimension when SI units are being used. Note that the three magnetic field components cannot be used as the three independent parameters since only two of them are independent following from the condition $\mathbf{k} \cdot \mathbf{B} = 0$. In this section we will see how the k-filtering method can be adjusted to include the magnetic and electric fields as measured by the STAFF and EFW instruments on Cluster.

[26] As we saw in section 3, the combination of STAFF and EFW measurements includes three components of the wave magnetic field, but only two components of the wave electric field. We call these components B_x, B_y, B_z, E_x and E_y, and we want to find a suitable constraining matrix for this situation. We find that there are two conditions that these measured components must satisfy. One is that the magnetic field must be divergence-free:

$$k_x B_x + k_y B_y + k_z B_z = 0, \quad (14)$$

and one follows from Faraday's law:

$$\omega B_z = k_x E_y - k_y E_x. \quad (15)$$

There are thus three independent quantities among the five that are measured here. The two conditions may be combined in order to obtain a constraining matrix for this

situation. As before, we put all the measured electromagnetic components into a five-component vector,

$$\mathbf{A}(\omega,\mathbf{k}) = \begin{pmatrix} E_x(\omega,\mathbf{k}) \\ E_y(\omega,\mathbf{k}) \\ cB_x(\omega,\mathbf{k}) \\ cB_y(\omega,\mathbf{k}) \\ cB_z(\omega,\mathbf{k}) \end{pmatrix}, \tag{16}$$

for simplification of notation.

[27] If we use E_x, E_y and B_x as the three independent components, we can write

$$\mathbf{A}(\omega,\mathbf{k}) = \mathbf{C_2}(\omega,\mathbf{k}) \begin{pmatrix} E_x \\ E_y \\ cB_x \end{pmatrix}, \tag{17}$$

where the constraining matrix $\mathbf{C_2}$ is given by

$$\mathbf{C_2}(\omega,\mathbf{k}) = \begin{pmatrix} 1 & 0 & 0 \\ 0 & 1 & 0 \\ 0 & 0 & 1 \\ \frac{k_z c}{\omega} & -\frac{k_x k_z c}{k_y \omega} & -\frac{k_x}{k_y} \\ -\frac{k_y c}{\omega} & \frac{k_x c}{\omega} & 0 \end{pmatrix}. \tag{18}$$

We note that some elements of this constraining matrix are not well defined for $k_y = 0$, so this matrix cannot be used for every possible $\mathbf{k}$. A similar complication occurs for $k_x = 0$ if we take E_x, E_y and B_y as the independent components.

[28] An alternative approach is to use E_x, E_y and E_z instead as the three independent components, even though E_z itself is not measured. This can be done since the three components to describe the wave field do not have to be the measured ones. In this case, equation (13) reduces into

$$\mathbf{A}(\omega,\mathbf{k}) = \mathbf{C_3}(\omega,\mathbf{k}) \begin{pmatrix} E_x(\omega,\mathbf{k}) \\ E_y(\omega,\mathbf{k}) \\ E_z(\omega,\mathbf{k}) \end{pmatrix}, \tag{19}$$

where the constraining matrix, $\mathbf{C_3}(\omega, \mathbf{k})$ is given by

$$\mathbf{C_3}(\omega,\mathbf{k}) = \begin{pmatrix} 1 & 0 & 0 \\ 0 & 1 & 0 \\ 0 & -\frac{ck_z}{\omega} & \frac{ck_y}{\omega} \\ \frac{ck_z}{\omega} & 0 & -\frac{ck_x}{\omega} \\ -\frac{ck_y}{\omega} & \frac{ck_x}{\omega} & 0 \end{pmatrix}. \tag{20}$$

The elements of this constraining matrix are well defined for all values of $\mathbf{k}$ in contrast to the case of $\mathbf{C_2}(\omega, \mathbf{k})$. There are other limitations for the use of $\mathbf{C_3}(\omega, \mathbf{k})$ as a constraining matrix, though. We saw in equation (7) that the matrix that is constructed by $\mathbf{C}^\dagger(\omega, \mathbf{k})\mathbf{H}^\dagger(\mathbf{k})\mathbf{M}^{-1}(\omega)\mathbf{H}(\mathbf{k})\mathbf{C}(\omega, \mathbf{k})$, must be invertible in order for the k-filtering technique to work. This implies that the rank of the constraining matrix must be the same as the number of independent components that are used. The constraining matrix $\mathbf{C_3}(\omega, \mathbf{k})$, that is given in equation (20), is of rank 3 in most cases, but it is of rank 2 when both k_x and k_y vanishes. In those cases only E_x and E_y are independent. This constraining matrix is used in the examples in section 6.

[29] A problem that is encountered in the k-filtering method when measurements of different types of physical parameters are combined, is that the numbers in the matrices may be of different orders of magnitude. This may lead to numerical instabilities during the analysis. In order to prevent these instabilities, we must normalize the data so that the numbers we put into the matrices are of comparable magnitude. For the Cluster data at hand, three magnetic and two electric field components, we define the ratio $R(\omega)$ by

$$R(\omega) = \frac{\left\langle \sqrt{|E_x(\omega)|^2 + |E_y(\omega)|^2} \right\rangle}{\left\langle \sqrt{|cB_x(\omega)|^2 + |cB_y(\omega)|^2 + |cB_z(\omega)|^2} \right\rangle}, \tag{21}$$

where the brackets denote the average over all spacecraft. We can then define a normalized wave field, $\tilde{\mathbf{A}}(\mathbf{r}, \omega)$, by

$$\tilde{\mathbf{A}}(\omega,\mathbf{r}) = \begin{pmatrix} E_x(\omega,\mathbf{r}) \\ E_y(\omega,\mathbf{r}) \\ R(\omega)cB_x(\omega,\mathbf{r}) \\ R(\omega)cB_y(\omega,\mathbf{r}) \\ R(\omega)cB_z(\omega,\mathbf{r}) \end{pmatrix}. \tag{22}$$

Using the same notation as before we can also define a normalized spatial correlation matrix, $\tilde{\mathbf{M}}(\omega)$, by

$$\tilde{\mathbf{M}}(\omega) = \left\langle \tilde{\mathbf{A}}(\omega)\tilde{\mathbf{A}}^\dagger(\omega) \right\rangle, \tag{23}$$

where $\tilde{\mathbf{A}}(\omega)$ is defined by

$$\tilde{\mathbf{A}}(\omega) = \begin{pmatrix} \tilde{\mathbf{A}}(\omega,\mathbf{r}_1) \\ \tilde{\mathbf{A}}(\omega,\mathbf{r}_2) \\ \vdots \\ \tilde{\mathbf{A}}(\omega,\mathbf{r}_N) \end{pmatrix}. \tag{24}$$

The number N is, as before, the number of spacecraft. With this normalization, Faraday's law takes the following form:

$$R(\omega)c\mathbf{B}(\omega,\mathbf{k}) = \frac{c\mathbf{k} \times \mathbf{E}(\omega,\mathbf{k})}{\omega/R(\omega)}, \tag{25}$$

from which it is easy to see that the normalized constraining matrix, $\tilde{\mathbf{C}}(\omega, \mathbf{k})$ is related to the unnormalized one, $\mathbf{C}(\omega, \mathbf{k})$, by

$$\tilde{\mathbf{C}}(\omega,\mathbf{k}) = \mathbf{C}(\omega/R(\omega),\mathbf{k}). \tag{26}$$

This relation is valid for all versions of the constraining matrix we have used here, and this fact simplifies the calculations. There is no need to modify the $\mathbf{H}(\mathbf{k})$ matrix to allow for the normalized wave field.

[30] With the normalization above, and with the notation we have introduced, we can use the k-filtering to obtain a normalized spectral density distribution, $\tilde{P}(\omega, \mathbf{k})$, given by

$$\tilde{P}(\omega,\mathbf{k}) = \mathrm{Tr}\left\{\tilde{\mathbf{C}}\left(\tilde{\mathbf{C}}^{\dagger}\mathbf{H}^{\dagger}\tilde{\mathbf{M}}^{-1}\mathbf{H}\tilde{\mathbf{C}}\right)^{-1}\tilde{\mathbf{C}}^{\dagger}\right\}. \quad (27)$$

The unnormalized spectral density distribution is then given by

$$P(\omega,\mathbf{k}) = \mathrm{Tr}\left\{\mathbf{D}(\omega)\tilde{\mathbf{P}}(\omega,\mathbf{k})\mathbf{D}(\omega)\right\}, \quad (28)$$

where $\tilde{\mathbf{P}}(\omega, \mathbf{k})$ is the normalized wave field energy matrix, the expression given between the brackets of equation (27), and where $\mathbf{D}(\omega)$ is defined by

$$\mathbf{D}(\omega) = \begin{pmatrix} 1 & 0 & 0 & 0 & 0 \\ 0 & 1 & 0 & 0 & 0 \\ 0 & 0 & 1/R(\omega) & 0 & 0 \\ 0 & 0 & 0 & 1/R(\omega) & 0 \\ 0 & 0 & 0 & 0 & 1/R(\omega) \end{pmatrix}. \quad (29)$$

We are thus able to retrieve the required spectral energy density distribution when using the normalized quantities.

[31] There are situations when the spacecraft are not identical for some reason or another, as we saw in section 3. We now examine how we can include such situations into the k-filtering framework. For this we assume that spacecraft 1 is the odd spacecraft, that only measures the magnetic field, $\mathbf{B}(\omega, \mathbf{k})$, and that the other three spacecraft measure both the magnetic field and two components of the electric field. We use the normalized expressions and put the measured quantities into one vector,

$$\tilde{\mathbf{A}}(\omega) = \begin{pmatrix} R(\omega)c\mathbf{B}(\omega,\mathbf{r}_1) \\ \tilde{\mathbf{A}}(\omega,\mathbf{r}_2) \\ \tilde{\mathbf{A}}(\omega,\mathbf{r}_3) \\ \tilde{\mathbf{A}}(\omega,\mathbf{r}_4) \end{pmatrix}, \quad (30)$$

which is the equivalent of equation (24), Here $\tilde{\mathbf{A}}(\omega, \mathbf{r})$ is defined as in equation (22). From this expression, we can define the spatial correlation matrix, $\tilde{\mathbf{M}}(\omega)$, exactly as in equation (23). The matrix $\mathbf{H}(\mathbf{k})$ must on the other hand be redefined to be able to handle the situation of non-identical spacecraft,

$$\mathbf{H}(\mathbf{k}) = \begin{pmatrix} \begin{pmatrix} 0 & 0 & 1 & 0 & 0 \\ 0 & 0 & 0 & 1 & 0 \\ 0 & 0 & 0 & 0 & 1 \end{pmatrix} e^{i\mathbf{k}\cdot\mathbf{r}_1} \\ \mathbf{I}_5 e^{i\mathbf{k}\cdot\mathbf{r}_2} \\ \mathbf{I}_5 e^{i\mathbf{k}\cdot\mathbf{r}_3} \\ \mathbf{I}_5 e^{i\mathbf{k}\cdot\mathbf{r}_4} \end{pmatrix}. \quad (31)$$

Using this matrix, we can perform the k-filtering when no constraints are included, as in equation (6). Some extra considerations have to be made in order to use the physical constraints also in this case.

[32] We can use the same constraining matrix as before for the satellites that measure the electric field. For the satellite with only magnetic field measurements, similar considerations gives us another constraint, $\mathbf{C_B}$, which must be based on the same three independent parameters. If E_x, E_y and E_z are used as the independent parameters, this constraint on the magnetic field measurements is given by

$$\begin{aligned} c\mathbf{B}(\omega,\mathbf{k}) &= \begin{pmatrix} 0 & -\frac{ck_z}{\omega} & \frac{ck_y}{\omega} \\ \frac{ck_z}{\omega} & 0 & -\frac{ck_x}{\omega} \\ -\frac{ck_y}{\omega} & \frac{ck_x}{\omega} & 0 \end{pmatrix} \begin{pmatrix} E_x(\omega,\mathbf{k}) \\ E_y(\omega,\mathbf{k}) \\ E_z(\omega,\mathbf{k}) \end{pmatrix} \\ &= \mathbf{C_B}(\omega,\mathbf{k}) \begin{pmatrix} E_x(\omega,\mathbf{k}) \\ E_y(\omega,\mathbf{k}) \\ E_z(\omega,\mathbf{k}) \end{pmatrix}, \end{aligned} \quad (32)$$

Note that even though we must use the same set of independent wave field components, we do not need to consider the rank of the matrix $\mathbf{C_B}(\omega, \mathbf{k})$ in the present analysis. We now introduce an additional matrix, $\mathbf{H}_{\tilde{\mathbf{C}}}(\omega, \mathbf{k})$, that can be seen as a combination of the matrices $\mathbf{H}(\mathbf{k})$ and $\tilde{\mathbf{C}}(\omega, \mathbf{k})$ that we have used before. This matrix is defined by

$$\mathbf{H}_{\tilde{\mathbf{C}}}(\omega,\mathbf{k}) = \begin{pmatrix} \mathbf{C_B}(\omega/R(\omega),\mathbf{k})e^{i\mathbf{k}\cdot\mathbf{r}_1} \\ \tilde{\mathbf{C}}(\omega,\mathbf{k})e^{i\mathbf{k}\cdot\mathbf{r}_2} \\ \tilde{\mathbf{C}}(\omega,\mathbf{k})e^{i\mathbf{k}\cdot\mathbf{r}_3} \\ \tilde{\mathbf{C}}(\omega,\mathbf{k})e^{i\mathbf{k}\cdot\mathbf{r}_4} \end{pmatrix}. \quad (33)$$

Using the above definitions, the k-filtering technique gives the normalized spectral density distribution as

$$\tilde{P}(\omega,\mathbf{k}) = \mathrm{Tr}\left\{\tilde{\mathbf{C}}\left(\mathbf{H}_{\tilde{\mathbf{C}}}{}^{\dagger}\tilde{\mathbf{M}}^{-1}\mathbf{H}_{\tilde{\mathbf{C}}}\right)^{-1}\tilde{\mathbf{C}}^{\dagger}\right\}, \quad (34)$$

and equation (28) can be used to calculate the unnormalized spectral density distribution, $P(\omega, \mathbf{k})$, from this expression. This derivation can of course easily be generalized to other situations where another spacecraft is lacking electric field data, or more than one spacecraft have the same problem.

5. Discussion of the Accuracy

[33] In order to be able to use the results from the k-filtering technique, we must examine the accuracy of the method. The reliability of the resulting estimates of the frequency wave vector spectra provided by this technique depends on factors such as the propagation of statistical errors in the data, the inaccuracy in the time synchronisation and in the inter-spacecraft distances, the time stationarity and space homogeneity of the measured data, the complexity of the measured fields and the spatial configuration of the satellites.

[34] Errors in the measurements of the electric and magnetic fields have obviously an effect on the quality of the spectra obtained from k-filtering. This has been studied in detail by *Pinçon and Lefeuvre* [1991] who also derived an expression for the stability of the estimation of the wave field energy distribution, $P(\omega, \mathbf{k})$. It can be expressed as a linear combination of the stability of the elements of the spatial correlation matrix, $\mathbf{M}(\omega)$, defined in equation (4). For a given frequency and a given wave vector the coefficients of this linear combination depend on the spatial

correlation matrix, the spatial configuration of the satellites and the value of $P(\omega, \mathbf{k})$. The main effect on the peaks of $P(\omega, \mathbf{k})$, evidenced by the k-filtering analysis, coming from statistical errors in the measured data is on their peak values. Their locations in wave vector space are not significantly altered. We will mainly focus on the locations in the examples in section 6.

[35] A possible source of error lies in imprecision of the relative positions of the spacecraft and in their time synchronization, and it may seriously affect the validity of the estimated wave field energy distribution. This topic has been studied by *Pinçon and Lefeuvre* [1992]. Inaccuracies in the time synchronization introduce phase shifts in the estimation of the power spectrum. If these phase shifts are in excess of a few degrees, the estimate of $P(\omega, \mathbf{k})$ may be distorted. On the Cluster mission, however, the wave magnetic and electric field measurements are provided with a time accuracy better than 1 ms. As we will only consider frequencies below 1 Hz in the data examples in the next section, it turns out that the phase shift we encounter due to time inaccuracy will always be smaller than 1°. We can consequently ignore time inaccuracy as a source of error in this study. The effect of inaccuracies in the inter-spacecraft distances can be evaluated from simulations. It has been shown to become noticeable when the relative errors of the distances are above 10%. This effect can be quantified by recalculating $P(\omega, \mathbf{k})$ repeatedly with random errors of the correct order introduced on the inter-spacecraft distances. The observed changes in the location in wave vector space for the main energy peak can be used to estimate the confidence intervals associated with these errors. The largest relative inaccuracy in spacecraft separation is found for the smallest inter-spacecraft distances, so this effect is most pronounced then.

[36] The validity of the wave field energy distribution provided by the k-filtering technique is based on the hypotheses of weak time stationarity and weak space homogeneity. It is difficult to predict the effects from the failure of these conditions. The time stationarity can be investigated using statistical tests. A statistical test of the space homogeneity is on the other hand not possible to perform in the frame of the Cluster mission. We can only verify that the same phenomena are observed on board each spacecraft. As a consequence there is no practical way to quantify the effect of this kind of errors and we have no other choice than to assume that the space homogeneity condition is satisfied.

[37] The resolution provided by the k-filtering technique depends on the number of measuring points, the number of field components used and the a priori information available. The validity of the obtained wave field energy distribution in wave vector space will also depend on the complexity of the fields that are analyzed. The more complex the field is, the more information has to be provided to the k-filtering technique. For the one-dimensional case, for instance, a field with a unique peak will be correctly characterized with only two spacecraft, but this cannot be done anymore as soon as we have more than one peak in the spectrum. This is demonstrated in Appendix A for the one-dimensional case. We will see that the number of intense peaks in our data examples for a given frequency is not too high. The main effect of having a more complex field is a decreasing resolution and an apparent enlargement of the peaks. The central positions of the peaks are not changed.

[38] Unambiguous determination of three-dimensional structures requires a three-dimensional spacecraft configuration. It is thus important to check that the Cluster configurations associated with our data sets are appropriate for the analysis. Two geometrical factors, the elongation E and the planarity P, have been defined as control parameters of the 3-D configuration [*Robert et al.*, 1998]. Values close to zero of these factors signifies the ideal 3-D configuration. In practice, even intermediate values of $P = 0.4$ and $E = 0.4$ still describe a good 3-D configuration. An effect arising from this problem is that the resolution in wave vector space gets a directional dependence.

6. Examples

[39] We now apply the k-filtering technique in the form derived in section 4 in two examples, where we use the wave magnetic and electric field data measured by the STAFF and EFW instruments on Cluster. The purpose of these examples is to examine the results that are obtained with k-filtering in different plasma environments and to better define the accuracy and limit of validity of the method as a function of different parameters as well as the number of wave components available.

6.1. First Example: Magnetosheath

[40] In the first example we use data that were obtained on 18 February 2002, between 05:34:00 and 05:36:44 UT. The reason to choose this time interval is that it has already been analyzed by *Sahraoui et al.* [2003, 2004] and *Walker et al.* [2004], which means that there are published results for the wave magnetic field data that can be used for comparison. The spacecraft are located in the inner magnetosheath, with an inter-spacecraft distance of about 100 km. The configuration has planarity $P = 0.05$ and elongation $E = 0.08$, which means that the satellites form an almost perfect regular tetrahedron. The outbound crossing of the magnetopause occurred at about 05:00 UT. The maximum in the energy distribution for each of the investigated frequencies in the spacecraft frame of reference has been found to be corresponding to a wave vector consistent with a Doppler shifted mirror mode [*Sahraoui et al.*, 2003]. The plasma bulk velocity with respect to the spacecraft is of the order of 220 km/s so the Doppler shift is considerable here. The electric field measurements from spacecraft 1 cannot be used for k-filtering during this time interval which means that equation (34) has to be utilized for the calculation of the wave energy distribution when the electric field measurements are included.

[41] The left panel of Figure 3 shows an iso-surface plot of the wave magnetic energy distribution, $P(\omega, \mathbf{k})$, for the frequency 0.61 Hz in the spacecraft frame of reference. This figure is obtained using only the magnetic field measurements together with the constraint $\mathbf{k} \cdot \mathbf{B} = 0$. The shown iso-surface corresponds to 30% of the maximum energy density for this frequency, and the wave vectors are calculated in the GSE coordinate system. This representation of the field energy distribution is useful to get an overview of where most of the wave energy is at a given frequency. The

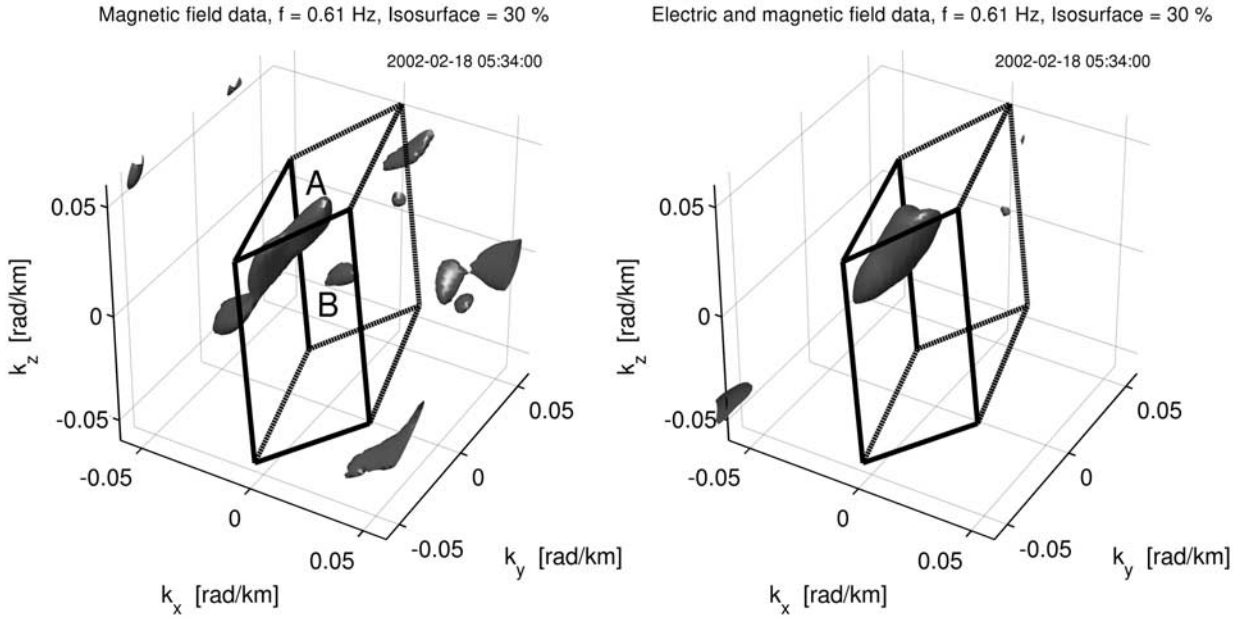

Figure 3. Iso-surface plots for the wave field energy distribution at 0.61 Hz in the spacecraft frame of reference for the data from 18 February 2002 05:34:00–05:36:44 UT. The left panel is calculated from the wave magnetic field measurements, and the electric field measurements are also included when the right panel is calculated. The displayed iso-surfaces correspond to 30% of the maximum wave energy density for this frequency. The box in the figure is included for visualization of the spatial aliasing properties. See color version of this figure in the HTML.

particular iso-level in the figure is chosen so that surface B is visible in the left panel. The box in the figure is included in order to visualize the spatial aliasing properties and is defined in section 2 (Figure 1). The right panel of Figure 3 shows the iso-surface of the normalized field energy distribution, $\tilde{P}(\omega, \mathbf{k})$, obtained using both the wave magnetic and electric fields in the calculations.

[42] The wave field energy distribution obtained using magnetic field measurements only, the left panel of Figure 3, is just the same as the one discussed by *Walker et al.* [2004]. This distribution was characterized by two maxima located at $\mathbf{k} \sim [-0.017, -0.0040, 0.0068]_{GSE}$ rad/km (inside the surface marked with A in the figure) and $\mathbf{k} \sim [0.019, -0.025, 0.030]_{GSE}$ rad/km (marked with B). We may actually find two different local maxima of the field energy distribution within surface A, but they were not considered as individual peaks of the energy density distribution in the previous study. This points out the problem whether to interpret two nearby local maxima as two distinct peaks or parts of a larger maximum, especially when these maxima are located inside an elongated iso-surface. The other surfaces, that are seen outside of the box in the figure, can be shown to correspond to peaks inside the box that have been subject to spatial aliasing.

[43] When we use both the magnetic and electric field measurements, as in the right panel of Figure 3, we immediately see that there are almost no aliased maxima visible. The important conclusion is that the effects of spatial aliasing are better surpressed in this case. We also note that the central surface is more smeared out. Further investigations of the wave energy density distribution show that this surface contains two energy maxima. The main energy peak is located within the upper part of the surface ($\mathbf{k} \sim [-0.014, -0.0016, 0.016]_{GSE}$ rad/km), and a secondary peak is found in the lower part ($\mathbf{k} \sim [-0.023, -0.0069, -0.0014]_{GSE}$ rad/km). An estimate of the error in the location of the main peak due to inaccuracies in the inter-spacecraft distances can be made following the ideas in section 5. This error is as small as $[\pm 0.0005, \pm 0.0002, \pm 0.0006]_{GSE}$ rad/km in this example. The location of both of these peaks is consistent with their interpretation as a Doppler shifted mirror mode [*Walker et al.*, 2004]. The energy level of the secondary peak is about 90% of that of the main peak and the energy level goes down to 70% between the two peaks, so it is clear that there is a significant amount of wave energy in the region around the secondary peak in the wave vector space. This peak, however, does not follow the strict definition from optics of a spectral line since the relative energy density does not go below 50% between the two peaks. The conclusion is thus that the notion of a sharp peak in wave vector space for the wave energy density distribution is not an accurate description. Instead we have a peak that is broadened in one direction and this must be remembered when discussing the position of the maximum energy density.

[44] We note that the main peak found in this example seems to correspond to the main peak in the study by *Walker et al.* [2004]. The secondary peak from the previous study is on the other hand almost perfectly suppressed when we use both wave magnetic and electric field data combined

Table 1. Wave Vectors in GSE Coordinates With the Highest Energy Density, Calculated for Four Frequencies in the Spacecraft Frame of Reference[a]

f_{sc}, Hz	k_x, rad/km	k_y, rad/km	k_z, rad/km	$\|\mathbf{k}\|$, rad/km	Difference in Norm	Difference in Direction
0.37	−0.01097	−0.00236	0.00528	0.01241	3%	7°
	−0.00988	−0.00228	0.00636	0.01197		
0.44	−0.01241	−0.00279	0.00529	0.01378	4%	28°
	−0.00896	−0.00185	0.01103	0.01433		
0.61	−0.01671	−0.00404	0.00682	0.01849	14%	28°
	−0.01372	−0.00164	0.01591	0.02107		
1.12	−0.03065	−0.00941	0.01438	0.03514	2%	10°
	−0.03245	−0.00773	0.00862	0.03445		

[a]The data are from 18 February 2002, 05:34:00–05:36:44 UT. The upper value for each frequency is calculated using k-filtering with only the wave magnetic field [from *Walker et al.*, 2004], and the lower one is calculated using k-filtering with both the electric and magnetic fields. The differences in norm and in the direction between the estimates are also included in the table.

with constraints. It is not visible even when we are investigating the 5% iso-surface level. It may, however, be found when no constraints are used. This suggests that the secondary peak observed by *Walker et al.* [2004] may come from aliasing effects, as discussed in section 2, since the aliased maxima are suppressed by the use of constraints. No peak has been found outside of the box, though, that can be this real maximum so other possibilities must be considered. The k-filtering technique assumes time stationarity of the data during the investigated time interval, but it was noted by [*Walker et al.*, 2004] that this is not really the case in this time interval. The importance of time stationarity is demonstrated in Appendix A. If the time interval in this example is divided into smaller parts the comparison between the results using and not using the electric field is better for each one of these subintervals, and the secondary peak is not clear in any one of them. The non-stationarity is then probably a source of the discrepancy between the results, and the previously identified secondary peak could therefore be incorrect. A conclusion is then that including the electric field measurements makes the k-filtering method less sensitive to artificially induced peaks thanks to more restrictive constraints on the wave field.

[45] The location in *k*-space for the wave energy density maximum has been calculated for four frequencies in the spacecraft frame of reference, using the k-filtering technique with both electric and magnetic field measurements. The results are shown in Table 1 where they are compared with the results from the previous study calculated using k-filtering but only the magnetic field measurements [*Walker et al.*, 2004]. We see that the inclusion of the electric field in the k-filtering makes small changes to the location of the maxima at these frequencies. For the chosen frequencies we find the largest discrepancy at 0.61 Hz, where the difference in norm of the wave vector is 14% and the difference in its direction is 28°. We may note that if we use the mean location of the two peaks we found at 0.61 Hz when including the electric field, the difference in direction is only 1°.

[46] A different way to visualize the results of k-filtering is to choose a plane in *k*-space in Figure 3 and show a two-dimensional iso-contour plot of the wave energy density in that plane. This has been done in Figure 4 for the planes with constant k_z going through the two energy density maxima we have found. The white lines are the iso-contours and the background color in the figure displays the ratio between the wave magnetic and electric field energy density, calculated from the diagonal elements of the wave field energy matrix $\mathbf{P}(\omega, \mathbf{k})$. Only the two measured electric field components are included in this ratio so the values may be misleading if most of the wave electric energy density has polarization along the satellite spin axis. The values of the ratio found here are at least of the same order of magnitude as they should be if the wave electric field measured by the spacecraft was solely due to magnetic field structures that are stationary in the plasma system of reference. This is consistent with the identification of these waves as Doppler shifted mirror modes. We see that the main energy maximum in this example has a stronger magnetic component than the secondary one, with ratios of $\sim$97 $(\mathrm{nT/(mV/m)})^2$ and $\sim$52 $(\mathrm{nT/(mV/m)})^2$. This difference in polarization makes it plausible that the secondary maximum is more difficult to detect when only magnetic field data are used. It may be difficult to draw conclusions from this kind of polarization analysis because of the missing electric field component and the fact that the spacecraft are moving with respect to the plasma. It is useful, however, to get an idea of the plasma physics involved in the observed wave modes. This investigation of the polarization could of course not be done without including electric field measurements.

6.2. Second Example: The Earth's Foreshock

[47] The data for the second example were obtained by the Cluster satellites on 29 February 2004 between 12:00:00 UT and 12:40:00 UT. The spacecraft were located in the foreshock during this time period, which has been chosen so that there are EFW electric field data available from all spacecraft during this time period and equations (27) and (28) can be used to find the wave energy distribution. The spacecraft have typical inter-spacecraft separation of about 200 km and their constellation has P = 0.49 and E = 0.41 which corresponds to a flattened tetrahedron. This constellation is not as ideal as in the first data example but it can still be used for k-filtering studies.

[48] An overview of the magnetic field for this time interval can be found in Figure 5. This figure shows the magnetic field measured by the Flux Gate Magnetometer (FGM) instrument [*Balogh et al.*, 1997] on all four spacecraft. We note that the time series for all four spacecraft are very similar, it is even difficult to discriminate the four

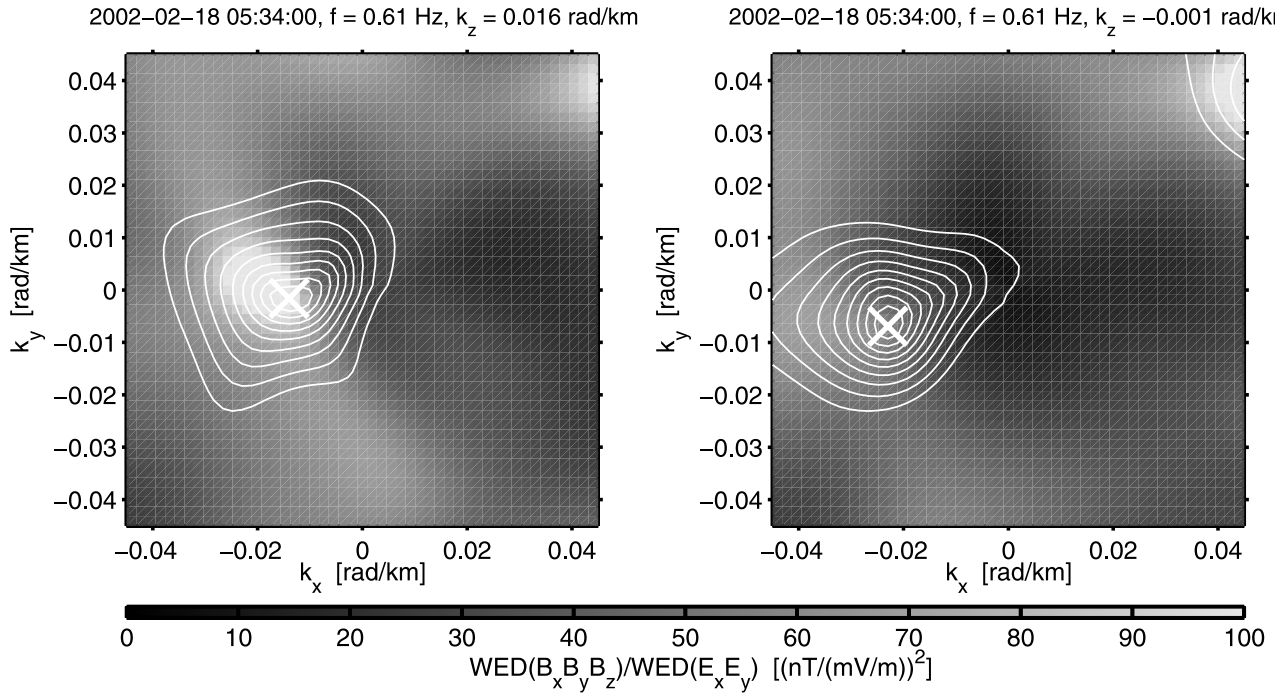

Figure 4. Contour plots for the wave energy density for the data from 18 February 2002, 05:34:00–05:36:44 UT. The background color denotes the ratio between the magnetic and the electric field energy density. The left panel displays the plane $k_z = 0.016$ rad/km and the right panel $k_z = -0.001$ rad/km. The crosses show the location in wave vector space for the local maxima in the energy density distribution. See color version of this figure in the HTML.

different time-series in any of the panels in the figure. We therefore assume space homogeneity. From this overview we see that there are two different plasma conditions that the spacecraft experience during this time period. One where the magnetic field fluctuations are small and another where these fluctuations are larger. These low frequency fluctuations are a common phenomenon in the Earth's foreshock region [*Greenstadt et al.*, 1995]. We focus on the time intervals marked in the figure as examples of these two different environments, and use the k-filtering technique with STAFF and EFW data to find differences between these two plasma conditions. Statistical tests prove that the data satisfy the time stationarity condition for both time intervals.

[49] The power spectral densities of the y_{GSE}-component of the magnetic field measured by the STAFF instrument on the four spacecraft are shown for the second time interval in Figure 6. We see that the spectra are very smooth without any clear peaks and also very similar between the spacecraft. We choose the frequency 0.42 Hz, marked in the figure, for further analysis. This choice of frequency is made because we want to analyze a frequency that is sufficiently low for the waves to have wavelengths larger than the typical spacecraft separation distance but also sufficiently high so that the high-pass filter with cut-off frequency 0.35 Hz, that is applied to the STAFF data, does not affect the analysis. The analysis has also been performed for other frequencies within this range with similar results.

[50] Figure 7 displays iso-surface plots of the wave energy density in *k*-space for the chosen frequency (0.42 Hz) in the spacecraft frame of reference. The left

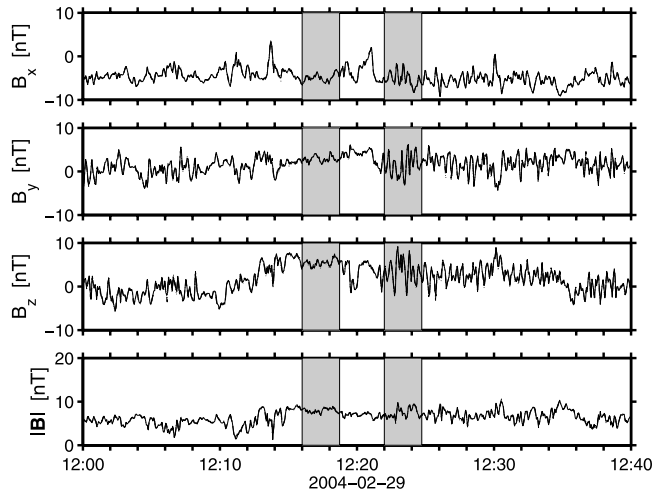

Figure 5. Overview of the magnetic field 29 February 2004 from 12:00:00 to 12:40:00 UT. These data are measured by the FGM instrument on all four spacecraft, and plotted with 4 s resolution. The panels are from top to bottom the *x*, *y*, *z* components of the magnetic field in GSE coordinates, and its magnitude. Spacecraft 1 is denoted by the solid, 2 by the dashed, 3 by the dash-dotted and 4 by the dotted line. The measured time series are so similar that it is difficult to discriminate the data from the individual satellites. The two marked time intervals are the ones that we focus on using the k-filtering technique. See color version of this figure in the HTML.

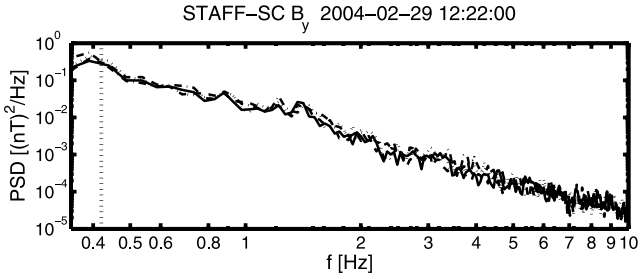

Figure 6. Power spectral densities of the y_{GSE}-component of the magnetic field measured by the STAFF instrument on the four Cluster satellites. The data are from the second marked time interval in Figure 5. The vertical line in the plot marks the frequency 0.42 Hz which is chosen for further analysis. See color version of this figure in the HTML.

panel shows the more quiet conditions (from 12:16:00 to 12:18:44 UT), and the right panel the more disturbed conditions (from 12:22:00 to 12:24:44 UT). The iso-surface level in this figure is 75% and is chosen in order to focus on the main peaks. We note that these two plots are quite similar, but they differ in some aspects. One difference is the location of the energy density maximum, which is at $\mathbf{k} \sim [-0.0018, 0.0037, -0.0034]_{GSE}$ rad/km for the first time interval, and $\mathbf{k} \sim [-0.0040, -8.5 \times 10^{-4}, -8.1 \times 10^{-4}]_{GSE}$ rad/km for the second one. There is a clear secondary peak in the wave energy distribution for the first time interval at $\mathbf{k} \sim [-0.0032, 3.7 \times 10^{-4}, -0.0058]_{GSE}$ rad/km with about 88% of the wave energy density of the maximum, but there is no such peak found during the second time interval. The additional surfaces that are seen outside of the boxes in the figure are due to the spatial aliasing phenomenon.

[51] If we instead study the polarization for the maxima in the wave energy density in the same way as in the previous example, there is a pronounced difference between the two time intervals. This can be seen in Figures 8 and 9, which are contour plots of the same type as Figure 4 except that the color scale is chosen differently for the polarization. Figure 8 shows the iso-contours for the data period 12:16:00–12:18:44 UT for $k_z = -0.003$ rad/km (the left panel) and for $k_z = -0.006$ rad/km (the right panel). We see that these two maxima have ratios between their wave magnetic and electric field energy densities of $\sim$2.0 (nT/(mV/m))^2 and $\sim$3.7 (nT/(mV/m))^2 respectively. Figure 9 is calculated for the data period 12:22:00–12:24:44 UT for $k_z = -0.001$ rad/km. The ratio is here $\sim$10.1 (nT/(mV/m))^2 so this wave mode has a larger magnetic component than the modes found during the calmer interval, but it is still small compared to the values found for the first example.

[52] An estimate of the error of the location in wave vector space of the main maximum due to inter-spacecraft distance inaccuricies, as described in section 5, has been made. It is $[\pm 0.0006, \pm 0.0005, \pm 0.0006]_{GSE}$ rad/km, so it is smaller than the separation between the two wave energy maxima. Since, in addition, the difference in their ratio of wave magnetic and electric field densities is quite large, it is reasonable to regard them as individual peaks in this discussion.

[53] The exact identification of the different wave modes and discussion of the physical mechanisms behind their presence in this plasma lie beyond the scope of the present article. We may make some reflections here though. Inspired by previous results [*Sahraoui et al.*, 2003], we investigate the location in the spacecraft frame of reference for a wave mode with vanishing frequency in the plasma rest frame of reference. Such mode can be viewed as magnetic field structures that are moving with the plasma. The large velocity of the plasma with respect to the

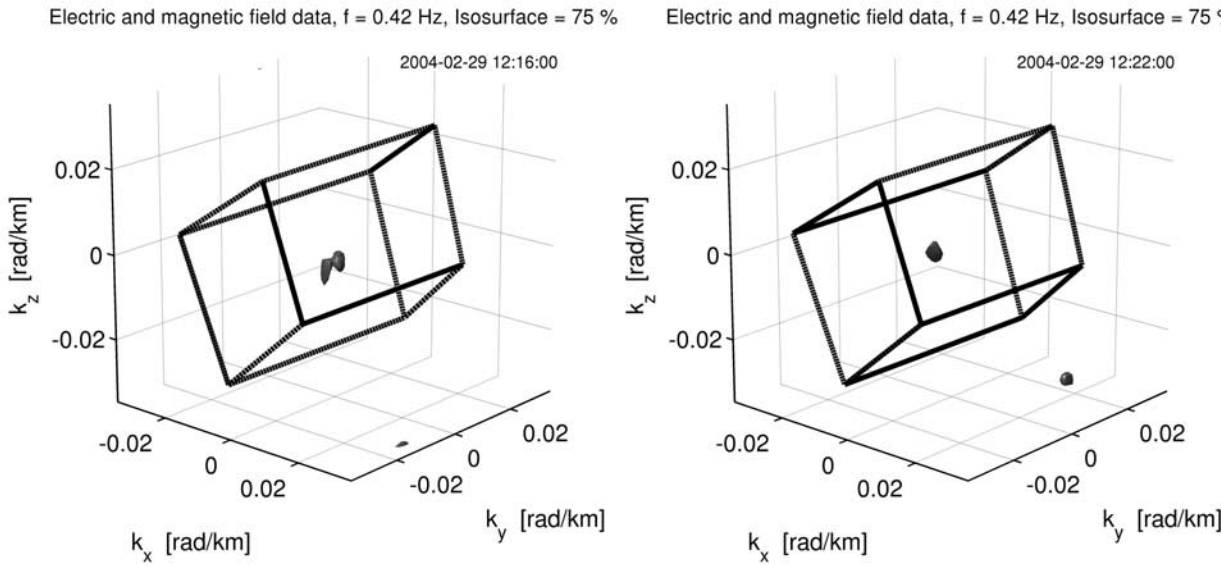

Figure 7. Iso-surface plots for 75% of the maximum wave energy density at 0.42 Hz for the data from 29 February 2004. The left panel is for the time period 12:16:00–12:18:44 UT and the right panel for the time period 12:22:00–12:24:44 UT. See color version of this figure in the HTML.

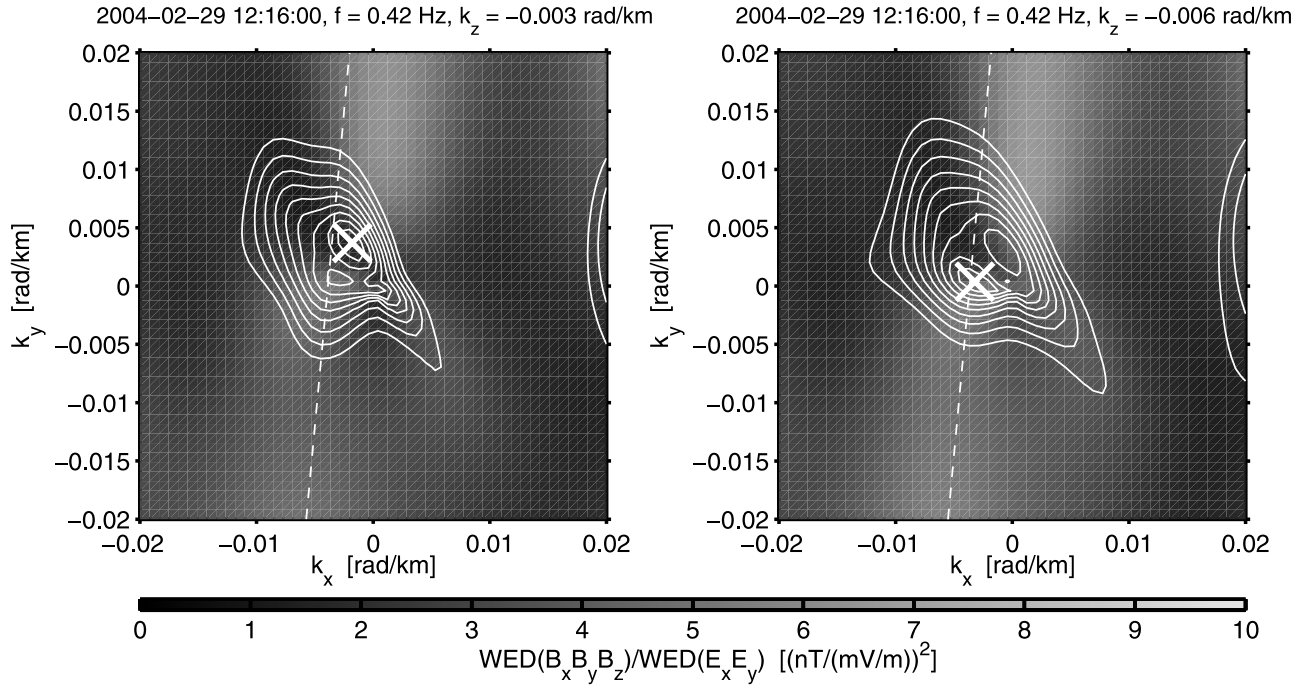

Figure 8. Contour plots of the same type as in Figure 4 for the data from 29 February 2004, 12:16:00–12:18:44 UT. The left panel shows the results for $k_z = -0.003$ rad/km and the right panel for $k_z = -0.006$ rad/km. The crosses mark the position of the maxima of the wave energy density. The dashed lines indicate the locations in the plots for a wave mode with vanishing frequency in the plasma frame of reference. See color version of this figure in the HTML.

spacecraft then gives rise to both the observed frequency spectrum and the electric field fluctuations in the spacecraft frame of references. The locations of non-propagating modes are indicated by dashed lines in Figures 8 and 9. We have used the mean plasma velocities measured by the CIS-CODIF instrument [*Rème et al.*, 2001] on spacecraft 4 for the calculations. They were $[-626, 58, -61]_{GSE}$ km/s and $[-617, 52, -55]_{GSE}$ km/s for the first and the second time interval respectively. The secondary maximum in the wave energy density from the first time interval and the peak from the second time interval lie almost perfectly on this line. This indicates that those two wave modes correspond to a non-propagating mode, or to a mode with very small phase velocity, in the plasma frame of reference.

[54] When we look at the main peak in the first time interval of this example, we note that it corresponds to the frequency 0.17 Hz in the plasma frame of reference. This may be compared with the proton gyro frequency in this plasma which is 0.12 Hz. The angle between the wave vector and the background magnetic field, calculated from its average during this time interval, is 89°. This peak thus corresponds to a wave mode that is propagating almost perpendicular to the background magnetic field with a frequency between the proton gyro frequency and its first harmonic in the plasma frame of reference. Combined with the small magnetic component and relatively small phase velocity (~20 km/s in the plasma frame of reference) we may conclude that this wave mode has the characteristics of a proton Bernstein mode [see, e.g., *Stix*, 1992]. This is, to our knowledge, the first indication of the existence of such waves in this region of space. The generating mechanisms

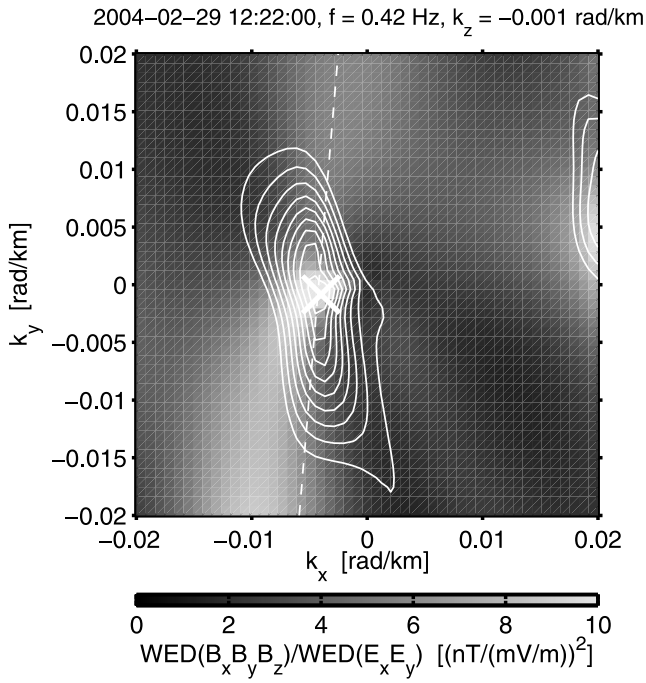

Figure 9. A plot of the same type as Figure 4 for the time period 12:22:00–12:24:44 UT and for $k_z = -0.001$ rad/km. The cross marks the position in wave vector space of the maximum of the wave energy density. The dashed line indicates the locations in the plot for a wave mode with vanishing frequency in the plasma frame of reference. See color version of this figure in the HTML.

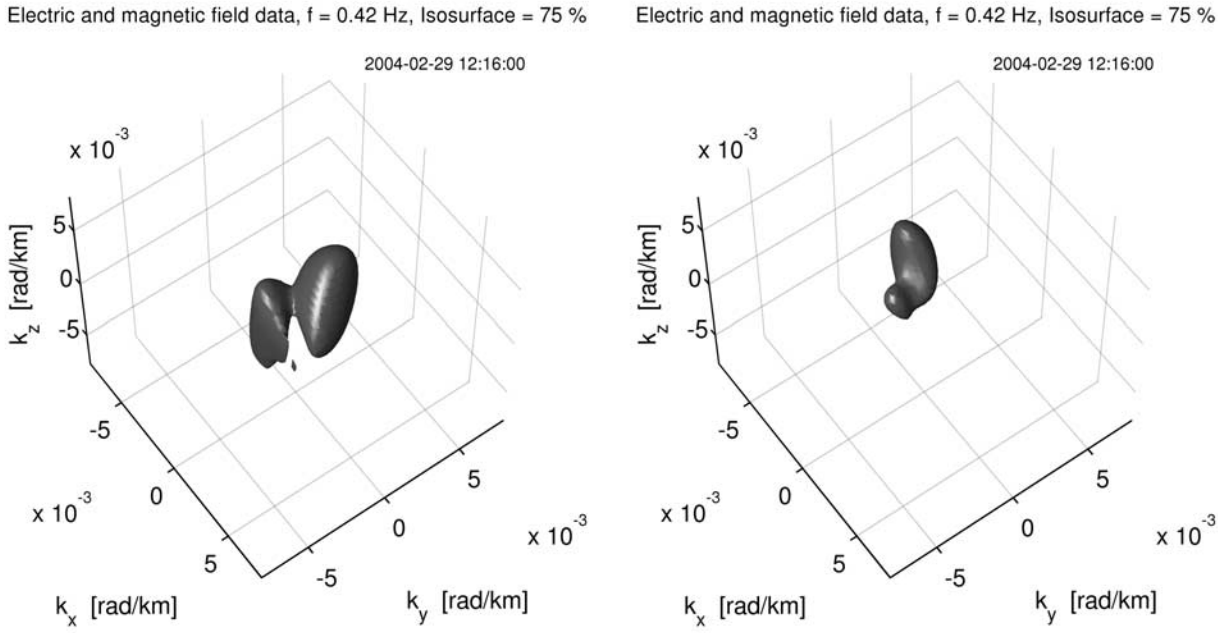

Figure 10. The left panel shows the central part of the left panel in Figure 7. The right panel shows the same region in *k*-space, but with the iso-surface calculated without using the electric field data from spacecraft 1. See color version of this figure in the HTML.

for such waves in this region are not clear, and could be the subject of further studies.

[55] One thing to note here is that the wave energy density distributions shown in Figure 8 are not symmetric along the dashed line in the figure, but they would be if the analysis had been done without using constraints. Such symmetry is expected if a non-propagating mode was the dominant wave mode in the plasma. During the first time interval in this example, the dominating wave is instead a propagating mode and the symmetry in the wave energy distribution is consequently not attained. In Figure 9, on the other hand, the dominating mode does indeed seem to be non-propagating so more of the symmetry is kept in the wave energy distribution.

[56] It is instructive to examine the effects on the result if the electric field measurements are removed from one satellite so that the situation resembles that of the first data example. The left panel of Figure 10 shows the central parts of the left panel of Figure 7, and we clearly see the main peak and the secondary peak. The right panel shows the same volume in *k*-space but the calculations are made without using the electric field measurements from satellite 1. The locations of the maxima are clearly shifted. This can be explained by the fact that the measured waves have a large electric component in this case, and hence the magnetic field measurements can be considered as background noise in the k-filtering analysis. We have then effectively reduced the data to only the three spacecraft with electric field measurements, and their two-dimensional configuration is not anymore adapted to the three-dimensional description of the wave field and we get higher sensitivity to errors, especially in the direction normal to the plane formed by these spacecraft. We thus see that the results of k-filtering have to be handled with care in cases when we have wave measurements with a dominating electric component in the spacecraft frame of reference combined with the lack of electric field measurements from one or more spacecraft. This effect is almost absent during the second time interval in this example, where the main wave mode has a larger magnetic component than during the first time interval. This brings us back to the first example (section 6.1) where we only used electric field measurements from three satellites. The secondary peak was not found in the previous study [*Sahraoui et al.*, 2003], and it was shown here to have a larger electric component than the main peak in that dataset. Its magnetic component is much larger than in the second time interval of the second example though. That together with the fact that, as we noted in section 6.1, the secondary peak can actually be found even when only magnetic field measurements are used makes us believe that our analysis of the first data example is valid.

[57] We finally note that the two wave modes during the first time period could not have been found without using a method that is capable of finding waves corresponding to more than one wave vector. The difference in polarization between these wave modes would not have been noticed if the electric field measurements had not been used.

7. Summary and Conclusions

[58] The k-filtering technique is a tool for investigating plasma waves in space, provided that we have multi-point measurements. We have for the first time used the combination of electric and magnetic field measurements in a study using the k-filtering technique. The data used in this study are from the EFW and STAFF instruments on the four

Cluster satellites and were obtained in the magnetosheath and in the foreshock. Things to note from the study include:

[59] 1. The k-filtering method has been extended to include electric field measurements from the EFW instrument. This means that the k-filtering equations have been modified to allow for measurements of only two electric field components. The method has also been modified to handle situations when electric field data from one or more satellites cannot be used. The two examples with Cluster data in this article could be analyzed thanks to these modifications of the technique.

[60] 2. The reason to include electric field data in the k-filtering is that we want as much data as possible to get the best estimate of the wave field energy distribution. More data channels also means that there are more constraints on the wave field that can be used so that the effects from spatial aliasing are diminished.

[61] 3. The inclusion of electric field measurements also enables some comparisons between the wave electric and magnetic parts of the wave energy density. These comparisons are useful in order to do some basic investigations of the polarization of the waves.

[62] 4. Having electric field measurements also makes it possible to detect waves where the electric field fluctuations are dominating. The main peak during the first time period in the second example of section 6 cannot be found when only wave magnetic field measurements are used.

[63] 5. Spacecraft induced perturbations in the electric field data can be reduced by using high-pass filtering in the satellite phase-angle domain. The stationarity constraints linked to this method are identical to those required by the k-filtering method.

[64] The method developed here was applied on magnetic and electric field data from an event in the magnetosheath. The results were then compared with those of a previous k-filtering study of the same event where only magnetic field data were used [*Sahraoui et al.*, 2003; *Walker et al.*, 2004]. At each studied frequency, the difference in location in wave vector space for the maximum of the wave energy distribution was found to be small between the studies. Discrepancies were found in the locations of the secondary peaks of the distribution, however, and a source of these discrepancies was assumed to be the non-stationarity of the data. An important point from the comparison between these two studies is that the effects from spatial aliasing are reduced when the electric field is included in the analysis. Another benefit from including the electric field data is that it enables comparisons between the electric and the magnetic energy densities of the waves. Electric field data from only three satellites were used in this example, and the wave electric field energy density was considerably less important than the magnetic. The spatial aliasing effects were reduced in spite of these facts, which shows that there are benefits from including the electric field measurements in the analysis even in cases such as this example. The conclusion from the previous study of this event, that the main energy maximum for each frequency corresponds to a Doppler shifted mirror mode, is not changed. It is even strengthened thanks to the reduced effects of spatial aliasing.

[65] Data from the foreshock region were analyzed as another example. The analysis showed the possible simultaneous presence of non-propagating modes and proton Bernstein modes in the plasma. It may be interesting to make a more detailed study of these waves, which would include particle data, so that their nature could be understood. The effects of excluding electric field data from one satellite from the analysis were also examined, and they were found to be significant in this example. This was due to the fact that the analysed wave data were dominated by electric fluctuations. The presented k-filtering analysis method should thus be used with caution in the cases when we have wave measurements with a large electric component and are using electric field measurements from less than four spacecraft.

[66] We have found that the k-filtering method including both magnetic and electric field measurements is a tool that is well-suited for identification and analysis of the waves that are encountered in the space plasma. There is still room for improvements of the method, though. Future work may include generalization of the method for the use of wavelets in order to reduce the requirement of stationarity of the time series. With the present method, we may extend the k-filtering studies from the Cluster satellites to frequencies below 0.35 Hz by using magnetic field data from the FGM instrument [*Balogh et al.*, 1997] combined with electric field data from the EFW instrument [*Gustafsson et al.*, 1997]. The technique can then be used on waves with wavelengths larger than in the present study which has already been done using FGM data only [*Eastwood et al.*, 2003; *Sahraoui et al.*, 2004], and it is thus not as dependent on having small spacecraft separation distances.

[67] Having this tool for wave mode identification provides a better understanding of the physics of the low frequency wave modes and instabilities in the plasma. This can be used in the magnetosheath for investigations of how information and energy are transported between the bow shock and the magnetopause, and how the plasma from the solar wind is modified before it enters the magnetosphere. The k-filtering technique also opens up possibilities to determine the spatial spectrum of the fluctuations in the plasma frame of reference, and this is of great interest for the evaluation of theories in space plasma turbulence.

Appendix A: Analytical Examples of k-Filtering

[68] Assume that $\phi(x, \omega)$ is a scalar wave field measured at the two points x_1 and x_2 in a one-dimensional space. In this case the matrix $\mathbf{H}(k)$ from equation (5) is a vector given by

$$\mathbf{H}(k) = \begin{pmatrix} e^{ikx_1} \\ e^{ikx_2} \end{pmatrix}, \tag{A1}$$

and the spatial correlation matrix, equation (4), is

$$\mathbf{M} = \left\langle \begin{pmatrix} \phi(x_1,\omega)\phi^*(x_1,\omega) & \phi(x_1,\omega)\phi^*(x_2,\omega) \\ \phi(x_2,\omega)\phi^*(x_1,\omega) & \phi(x_2,\omega)\phi^*(x_2,\omega) \end{pmatrix} \right\rangle. \tag{A2}$$

The symbol * denotes complex conjugation. We apply the k-filtering technique to some simple analytical examples of wave fields.

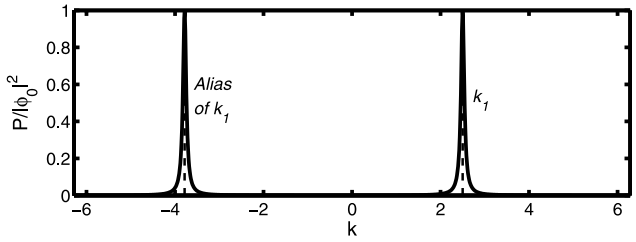

Figure A1. Analytical example of the k-filtering technique. The wave field is assumed to consist of a single monochromatic wave with $k = 2.5$ with a small amount of incoherent noise added to the signal. We are using data from two spacecraft positioned at $x = 0$ and $x = 1$. The effect of spatial aliasing is clearly seen as a spurious peak at $k \sim -3.8$. See color version of this figure in the HTML.

[69] In the first example we have a single monochromatic wave component with frequency ω and wave number k' so that the wave can be denoted by $\phi(x, \omega) = \phi_0 e^{ik'x}$. This leads to a spatial correlation matrix which is given by

$$\mathbf{M} = |\phi_0|^2 \begin{pmatrix} 1 & e^{ik'(x_1-x_2)} \\ e^{ik'(x_2-x_1)} & 1 \end{pmatrix}. \tag{A3}$$

The k-filtering technique involves an inversion of this matrix as we saw in equation (6), but this matrix is not invertible in the present case. This problem can be resolved if we introduce a small amount of incoherent noise in the signal. This adds a small number, $\varepsilon \ll 1$, to the diagonal elements of the spatial correlation matrix $\mathbf{M}(\omega)$ which now becomes

$$\mathbf{M} = |\phi_0|^2 \begin{pmatrix} 1+\varepsilon & e^{ik'(x_1-x_2)} \\ e^{ik'(x_2-x_1)} & 1+\varepsilon \end{pmatrix}. \tag{A4}$$

The matrix inversion can now be performed and we find

$$\mathbf{M}^{-1} = \frac{1}{|\phi_0|^2\varepsilon(2+\varepsilon)} \begin{pmatrix} 1+\varepsilon & -e^{ik'(x_1-x_2)} \\ -e^{ik'(x_2-x_1)} & 1+\varepsilon \end{pmatrix}. \tag{A5}$$

We can now use equation (6) to calculate an estimate of the wave energy density:

$$P(k) = \frac{|\phi_0|^2\varepsilon(2+\varepsilon)}{2(1+\varepsilon-\cos[(k'-k)(x_1-x_2)])}. \tag{A6}$$

An example with the two spacecraft positioned at $x_1 = 0$ and $x_2 = 1$ and where $k' = 2.5$ is shown in Figure A1. We note that $P(k') = |\phi_0|^2(1 + \varepsilon/2) \approx |\phi_0|^2$ since ε is assumed to be much smaller than 1. This means that all the wave power passes the filter for $k = k'$, exactly as it is designed to do. Furthermore, $P(k) < |\phi_0|^2$ for $k' \neq k$ and it can be shown that the peak in the power distribution is sharper for smaller values of ε. In addition, we note that the wave power distribution in equation (A6) is periodic in k which manifests in a spurious peak that is seen at $k \sim -3.8$ in Figure A1. This is an example of the spatial aliasing problem that was discussed in section 2.

[70] Our second example is a wave field that consists of two monochromatic wave components with the same frequency, ω, but with different wave numbers, k_1' and k_2'. This wave field can be denoted by $\phi(x) = \phi_1 e^{ik'_1 x} + \phi_2 e^{ik'_2 x}$ and the elements of the spatial correlation matrix that this wave field gives rise to are

$$\begin{aligned}
M_{11} &= |\phi_1|^2 + \phi_1\phi_2^* e^{i\left(k_1'-k_2'\right)x_1} + \phi_2\phi_1^* e^{i\left(k_2'-k_1'\right)x_1} + |\phi_2|^2 \\
M_{12} &= |\phi_1|^2 e^{ik_1'(x_1-x_2)} + \phi_1\phi_2^* e^{i\left(k_1'x_1-k_2'x_2\right)} + \phi_2\phi_1^* e^{i\left(k_2'x_1-k_1'x_2\right)} \\
&\quad + |\phi_2|^2 e^{ik_2'(x_1-x_2)} \\
M_{21} &= |\phi_1|^2 e^{ik_1'(x_2-x_1)} + \phi_1\phi_2^* e^{i\left(k_1'x_2-k_2'x_1\right)} + \phi_2\phi_1^* e^{i\left(k_2'x_2-k_1'x_1\right)} \\
&\quad + |\phi_2|^2 e^{ik_2'(x_2-x_1)} \\
M_{22} &= |\phi_1|^2 + \phi_1\phi_2^* e^{i\left(k_1'-k_2'\right)x_2} + \phi_2\phi_1^* e^{i\left(k_2'-k_1'\right)x_2} + |\phi_2|^2.
\end{aligned} \tag{A7}$$

Here we have assumed, as in the previous example, that we have two spacecraft positioned at x_1 and x_2 respectively. We see that the elements M_{11} and M_{22} in general depend on the choice of origin which ultimately means that the spectral energy density would contain a spatial dependence. However, this dependence disappears in cases when $\phi_1\phi^*{}_2 e^{i(k'_1-k'_2)x_{1,2}} = -\phi_2\phi^*{}_1 e^{i(k'_2-k'_1)x_{1,2}}$ is satisfied. This can only happen for $k_1' = k_2'$ which means that there would in effect be only one plane wave present and the results from the previous example can be used.

[71] If we instead have two plane waves $\phi_1(x)$ and $\phi_2(x)$, with wave numbers k_1' and k_2' respectively, that are not phase-coherent, the mixed terms of the elements of the spatial correlation matrix are removed by the averaging process made in the definition from equation (4). We can then create the total correlation matrix by adding the spatial correlation matrices of the individual waves which removes the spatial dependence of the spectral density. These calculations, except for a factor 1/2, are also valid for a situation where we have a wave field consisting of $\phi_1(x)$ for one half of the time interval and $\phi_2(x)$ for the other half. This example thus also demonstrates a situation where we do not have time stationary data. The elements of the spatial correlation matrix are then given by

$$\begin{aligned}
M_{11} &= |\phi_1|^2 + |\phi_2|^2 \\
M_{12} &= |\phi_1|^2 e^{ik_1'(x_1-x_2)} + |\phi_2|^2 e^{ik_2'(x_1-x_2)} \\
M_{21} &= |\phi_1|^2 e^{ik_1'(x_2-x_1)} + |\phi_2|^2 e^{ik_2'(x_2-x_1)} \\
M_{22} &= |\phi_1|^2 + |\phi_2|^2,
\end{aligned} \tag{A8}$$

in this example. We find after some algebra that the k-filtering estimate of the wave energy density distribution for this example is given by

$$P(k) = \frac{|\phi_1|^2|\phi_2|^2\left(1-\cos\left[\left(k_1'-k_2'\right)(x_1-x_2)\right]\right)}{|\phi_1|^2(1-\cos\kappa_1)+|\phi_2|^2(1-\cos\kappa_2)}, \tag{A9}$$

where $\cos\kappa_i = \cos[(k_i' - k)(x_1 - x_2)]$. We note that $P(k_1') = |\phi_1|^2$ and $P(k_2') = |\phi_2|^2$ which is exactly what the filter is designed to give. There is, however, only one peak in the spectral density, except from the spurious ones arising from spatial aliasing, and it is neither at $k = k_1'$ nor at $k = k_2'$, as we can see in the upper panel of Figure A2. That figure shows the wave energy density distribution for $k_1' = 2.5$ and $k_2' = 0.2$ measured by two spacecraft positioned at $x_1 = 0$ and

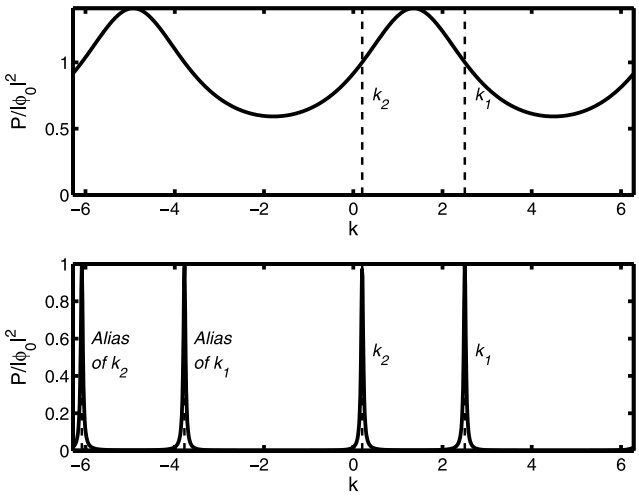

Figure A2. Analytical example of the k-filtering technique. The wave field is assumed to consist of two monochromatic waves with the same frequency and amplitude $|\phi_0|$, and these two wave modes have the wave numbers $k = 2.5$ and $k = 0.2$ respectively. In the upper panel we are using data from two spacecraft at $x = 0$ and $x = 1$ and in the lower panel we have added a third spacecraft at $x = 2$. It is clear that the two wave modes cannot be resolved in the first of these cases. The effect of the spatial aliasing can once again bee seen as a periodicity in the wave energy distribution. See color version of this figure in the HTML.

$x_2 = 1$. We can thus only find one wave mode using two spacecraft in a one-dimensional space, which is what we observed in section 2 about the number of observable wave modes using the k-filtering technique. Following that discussion, it would be possible to increase the number of observable modes either by increasing the number of wave components measured on each spacecraft or by increasing the number of spacecraft. This is indeed the case, and the bottom panel of Figure A2 displays the result for the same wave field as that of the upper panel but with an added spacecraft positioned at $x_3 = 2$. It is therefore clear that it is important to include as much data as possible in the k-filtering in order to obtain the best results. We have also seen the importance of time stationarity in the data.

[72] **Acknowledgments.** This work was partially supported by the European Community's Human Potential Programme under contract HPRN-CT-2001-00314 "Turbulent Boundary Layers in Geospace Plasmas." The background magnetic field data were provided by the FGM instrument team (E. Lucek). The ion data were provided by the CIS instrument team (H. Rème).

[73] Shadia Rifai Habbal thanks Jonathan Eastwood and another referee for their assistance in evaluating this paper.

References

Balogh, A., et al. (1997), The Cluster magnetic field investigation, *Space Sci. Rev.*, *79*, 65–91.

Capon, J. (1969), High-resolution frequency-wavenumber spectrum analysis, *Proc. IEEE*, *57*(8), 1408–1418.

Carozzi, T. D., A. M. Buckley, and M. P. Gough (2004), Instantaneous local wave vector estimation from multi-spacecraft measurements using few spatial points, *Ann. Geophys.*, *22*(7), 2633–2641.

Cornilleau-Wehrlin, N., et al. (1997), The Cluster spatio-temporal analysis of field fluctuations (STAFF) experiment, *Space Sci. Rev.*, *79*, 107–136.

Dudok de Wit, T., V. V. Krasnosel'skikh, S. D. Bale, M. W. Dunlop, H. Lühr, S. J. Schwartz, and L. J. C. Woolliscroft (1995), Determination of dispersion relations of quasi-stationary plasma turbulence using dual satellite data, *Geophys. Res. Lett.*, *22*(19), 2653–2656.

Dunlop, M. W., D. J. Southwood, K.-H. Glassmeier, and F. M. Neubauer (1988), Analysis of multipoint magnetometer data, *Adv. Space Res.*, *8*(9–10), 273–277.

Eastwood, J. P., A. Balogh, E. A. Lucek, C. Mazelle, and I. Dandouras (2003), On the existence of Alfvén waves in the terrestial foreshock, *Ann. Geophys.*, *21*(7), 1457–1465.

Escoubet, C. P., R. Schmidt, and M. L. Goldstein (1997), Cluster — Science and mission overview, *Space Sci. Rev.*, *79*, 11–32.

Glassmeier, K.-H., et al. (2001), Cluster as a wave telescope—First results from the fluxgate magnetometer, *Ann. Geophys.*, *19*, 1439–1447.

Greenstadt, E. W., G. Lee, and R. J. Strangeway (1995), ULF waves in the foreshock, *Adv. Space Res.*, *15*(8/9), 71–84.

Gustafsson, G., et al. (1997), The electric field and wave experiment for the Cluster mission, *Space Sci. Rev.*, *79*, 137–156.

Neubauer, F. M., and K.-H. Glassmeier (1990), Use of an array of satellites as a wave telescope, *J. Geophys. Res.*, *95*(A11), 19,115–19,122.

Pedersen, A., F. Mozer, and G. Gustafsson (1998), Electric field measurements in a tenuous plasma with spherical double probes, in *Measurement Techniques in Space Plasmas*, *Geophys. Monogr.*, vol. 103, edited by J. Borovsky, R. Pfaff, and D. Young, pp. 1–12, AGU, Washington, D. C.

Pinçon, J. L., and F. Lefeuvre (1991), Local characterization of homogeneous turbulence in a space plasma from simultaneous measurements of field components at several points in space, *J. Geophys. Res.*, *96*(A2), 1789–1802.

Pinçon, J. L., and F. Lefeuvre (1992), The application of the generalized Capon method to the analysis of a turbulent field in space plasma: Experimental constraints, *J. Atmos. Terr. Phys.*, *54*(10), 1237–1247.

Pinçon, J.-L., and U. Motschmann (1998), Multi-spacecraft filtering: General framework, in *Analysis Methods for Multi-Spacecraft Data*, edited by G. Paschmann and P. W. Daly, *ISSI Sci. Rep., SR-001*, chap. 3, pp. 65–78.

Rème, H., et al. (2001), First multispacecraft ion measurements in and near the Earth's magnetosphere with the identical Cluster ion spectrometry (CIS) experiment, *Ann. Geophys.*, *19*, 1303–1354.

Robert, P., A. Roux, C. C. Harvey, M. W. Dunlop, P. W. Daly, and K.-H. Glassmeier (1998), Tetrahedron geometric factors, in *Analysis Methods for Multi-Spacecraft Data*, edited by G. Paschmann and P. W. Daly, *ISSI Sci. Rep., SR-001*, chap. 13, pp. 323–348.

Sahraoui, F., et al. (2003), ULF wave identification in the magnetosheath: k-filtering technique applied to Cluster II data, *J. Geophys. Res.*, *108*(A9), 1335, doi:10.1029/2002JA009587.

Sahraoui, F., G. Belmont, J. L. Pinçcon, L. Rezeau, A. Balogh, P. Robert, and N. Cornilleau-Wehrlin (2004), Magnetic turbulent spectra in the magnetosheath: New insights, *Ann. Geophys.*, *22*(6), 2283–2288.

Samson, J. C. (1983), Pure states, polarized waves and principal components in the spectra of multiple geophysical time series, *Geophys. J. R. Astron. Soc.*, *72*, 647–664.

Schwartz, S. J., D. Burgess, and J. J. Moses (1996), Low-frequency waves in the Earth's magnetosheath: Present status, *Ann. Geophys.*, *14*(11), 1134–1150.

Stenberg, G., T. Oscarsson, M. André, and C. C. Chaston (2002), Investigating data wave data from the FAST satellite by reconstructing the wave distribution function, *J. Geophys. Res.*, *107*(A8), 1190, doi:10.1029/2001JA900154.

Stix, T. H. (1992), *Waves in Plasmas*, Am. Inst. of Phys., New York.

Storey, L. R. O., and F. Lefeuvre (1979), The analysis of 6-component measurements of a random electromagnetic wave field in a magnetoplasma— I. The direct problem, *Geophys. J. R. Astron. Soc.*, *56*, 255–269.

Walker, S. N., F. Sahraoui, M. A. Balikhin, G. Belmont, J. L. Pinçon, L. Rezeau, H. Alleyne, N. Cornilleau-Wehrlin, and M. André (2004), A comparison of wave mode identification techniques, *Ann. Geophys.*, *22*(8), 3021–3032.

M. André and F. Sahraoui, Swedish Institute of Space Physics, Box 537, 751 21 Uppsala, Sweden. (mats.andre@irfu.se; fouad.sahraoui@cetp.ipsl.fr)

N. Cornilleau-Wehrlin, CETP/IPSL, 10–12 Avenue de l'Europe, 78140 Vélizy, France. (nicole.cornilleau@cetp.ipsl.fr)

J.-L. Pinçon and A. Tjulin, LPCE/CNRS, 3A Avenue de la Recherche Scientifique, 45071 Orléans, France. (jlpincon@cnrs-orleans.fr; a.tjulin@imperial.ac.uk)